

Effect of Conductor YZ–Inclination Angle on the Quality of Conductor Positioning and Confinement for the Superconducting Magnet Ends

S. Yadav

*Fermi National Accelerator Laboratory
MS 316, PO Box 500, Batavia, IL, USA*

1. Introduction

As a next logical step on energy frontier after the Large Hadron Collider (LHC), Fermilab is involved in conducting R&D work for a future Very Large Hadron Collider (VLHC) with 100 TeV center-of-mass energy and 10^{34} cm⁻²s⁻¹ luminosity, using superconducting magnets of very high fields (11-12 T). One of the main challenges for the feasibility of such a future collider is to make technological advances and to find cost reduction strategies to significantly reduce the overall cost of the machine. Since superconducting magnets are the most costly and technically challenging components of a hadron collider, a large effort is being made to optimize magnet design between cost and performance. Also, since Fermilab has a large body of experience and developed tooling from building NbTi cosine-theta magnets for the Tevatron and LHC, efforts are directed towards utilizing this existing expertise and tooling for building high field Nb₃Sn magnets in a two-layer cosine-theta structure. It should be noted that a cosine-theta design is the most efficient one in its use of superconductor, iron and steel; materials that add significantly to the overall cost of a superconducting magnet. Another major cost driving factor is the coil end parts that should provide sufficient support to the conductors at the ends. Alternate magnet designs based on the common coil methodology have been proposed with the presumed potential of significantly reducing the cost of the magnets due to their relatively simple design of two-dimensional end spacers and wedges. However, as discussed later in this paper, recent technological advances in the manufacturing processes have made it possible to fabricate coil end parts for the cosine-theta design at a very economical and competitive price.

Current Fermilab efforts are focused on making a dipole of 43.5 mm bore diameter. It should be noted that for a 100 TeV machine, very large head loads due to synchrotron radiation are expected. In order to reduce the cryogenic power consumption, it would be necessary to have a beam screen inside the cold bore that would be operated at some

intermediate higher temperature. Besides their primary function of intercepting beam-induced heat loads by sheltering the cold bore surface from synchrotron radiation, the beam screen prevents desorption of the adsorped gas molecules, thereby avoiding the breakdown of the beam vacuum [1]. The space required for the beam screen, its cooling tubes [2], and the necessary clear beam aperture imposes a practical limit to the minimum bore size. We believe that the optimum bore size would be somewhere between 40-50 mm.

Fig. 1 shows the cross-section of the first dipole model. The coil end parts are designed using program BEND developed by Joe Cook of Fermilab. Before presenting specific design details for the coil end parts, we present a brief introduction to the salient features of program BEND.

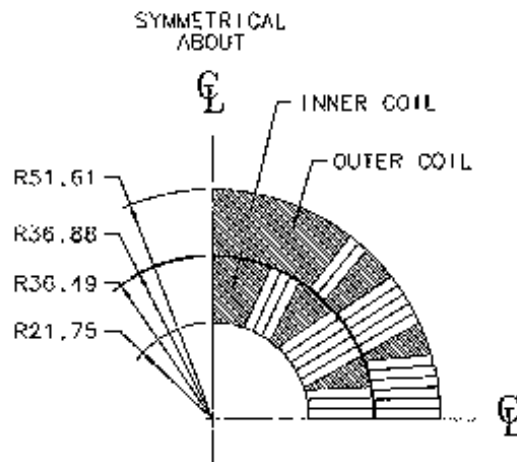


Fig. 1. Cross-section view of the first dipole model magnet.

Figure 1: Cross-section of the first dipole model. The coil is made of two-layers without any interlayer splice.

2. Program BEND

Program BEND is based on alignment of conductors on the outside radius of the layer. First, a base curve on the outside radius is obtained that minimizes the elastic strain energy of bending of the curve. This minimization is based on the classical works on large deflection of linearly elastic beams by Jacob Bernoulli, Euler, Lagrange, and Plana with the added constraint that the base curve is required to lie on the surface of a cylinder. This gives rise to a fourth order linear ordinary differential equation whose solution is determined by four end point boundary conditions. In program BEND, the boundary conditions are split between the two end-points, two at each end where the position of each end-point and the tangent to the base curve at that end-point are imposed. Program BEND then solves the differential equation iteratively using a two-dimensional Regula Falsi technique.

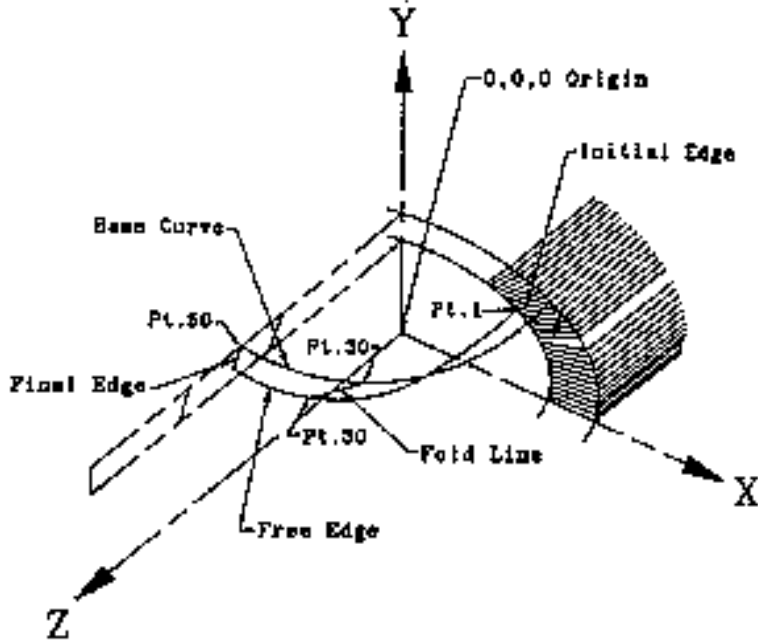


Figure 2: The rectifying developable surface (from Reference 5).

Once the base curve is obtained, the other edge (called as free edge) of the conductor is obtained to model a thin strip of conductor surface bent around a cylindrical surface (see Fig. 2). This free edge is obtained based on the concept of a rectifying developable surface, which implies that the strip bent around the cylindrical surface could be folded flat on a planar surface. This leads to a surface of minimum strain energy within the given constraints. Program BEND uses fifty points on the base curve (equally spaced angularly) and obtains ruling vectors ($\vec{\delta}$) at each of these points given by:

$$\vec{\delta} = \tau \vec{T} + \kappa \vec{B}, \quad (1)$$

where τ is the torsion and κ the curvature of the base curve, \vec{T} is a vector that is tangent to the base curve in the direction of increasing arc length, and \vec{B} is the binormal vector to the base curve obtained using $\vec{B} = \vec{T} \times \vec{N}$, where \vec{N} is the normal vector to the base curve. It should be noted that the ruling vector at the point with maximum Z-coordinate (point 50 in Fig. 2) establishes the final edge angle of the strip. It could also be shown mathematically that the ruling vector at $Z = 0$ is perpendicular to the cylinder. However, the angle of inclination of the cable along the straight section of the coil winding is generally not the same as that given by the ruling vector at $Z = 0$. Therefore, the rectifying developable strip is twisted by rotating its rulings about \vec{T} until the twisted strip joins smoothly with the strip as given along the straight section of the coil winding. This twist is distributed smoothly along the complete arc length, with an option to change this distribution using user-defined inputs. It should be noted that this causes deviation from the rectifying developable surface and hence a violation of the constant perimeter conditions, causing some hard-way bending in the strip. A detailed mathematical description of these concepts can be found in [3], [4].

3. Cable Shape Change

As a Rutherford cable with a keystone angle is wrapped around the end parts, a de-keystoning of the cable along with an accompanying increase in the cable mid-thickness is observed. Program BEND has two parameters that allow the user to quantitatively specify the degree of de-keystoning and increase in cable mid-thickness as shown in Fig. 3.

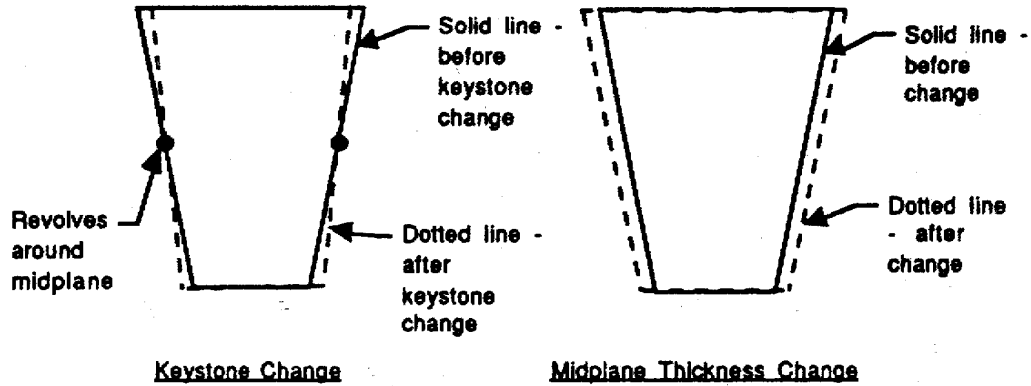


Figure 3: Schematic representation of de-keystoning and increase in cable mid-thickness during winding around the magnet end parts (from Reference 6).

The program lets the user specify these cable shape change parameters at two locations: first at the middle of the arc length of the base curve and second at the end (maximum Z) of the base curve. The intermediate values of the cable shape change parameters are computed by the program using a linear interpolation fit. The stacking of the conductors in a given current group is then performed using the grouped method approach where the turns within each conductor block are laid directly on each other with no spaces between them. The advantage of this grouped method approach is that the spaces between the turns are eliminated.

4. Effect of Conductor YZ-Inclination Angle

Fig. 4 shows the YZ cross-sections of the lead and return ends of the Fermilab dipole magnet. The inclination angle from the vertical axis of the conductor in the YZ plane, also called as the final edge angle, is a parameter that can be varied within program BEND. Generally, the final edge angle obtained from program BEND increases for the conductor groups that are closer to the midplane. Please see Tables 1-4 that provide the conductor inclination angles obtained using program BEND for the different conductor groups shown in Fig. 4. It should be noted that the final edge angle obtained from program BEND is based upon a rectifying developable surface (that is twisted by a small angle to match the inclination angle of the conductor in the straight section), and therefore represents a configuration of minimum strain energy. However for large final edge angles, gaps appear on the inside radius. This happens because the cables are laying at an angle and no longer require as much radial clearance as they would if they were

stacked vertically. Fermilab has tackled this problem in the past by having a shelf as an integral part of an end spacer (Fig. 5), attached at the inside radius and thus filling the empty space. This approach has worked well for Fermilab as evidenced by the fact that most of the quenches observed in the model high gradient quadrupole (HGQ) magnets built as part of the LHC Interaction Region Quadrupole program were in the straight section and not at the magnet ends. This shows that the conductors were well confined at the ends.

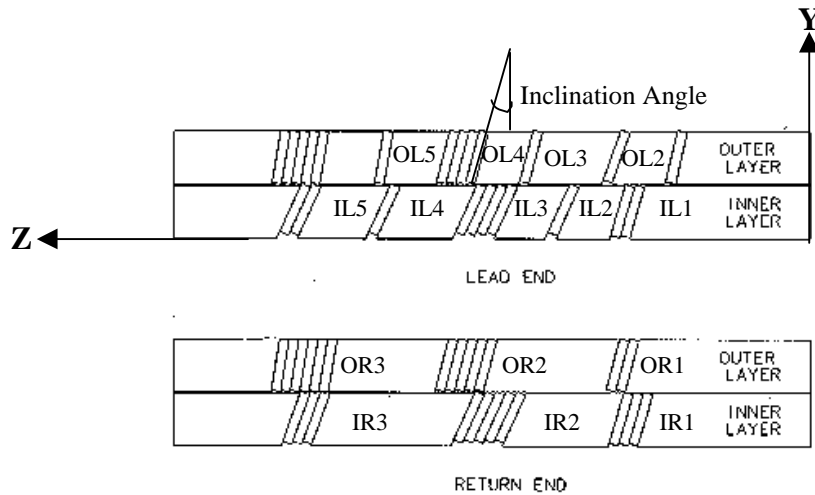


Figure 4: Lead end and return end cross-sections.

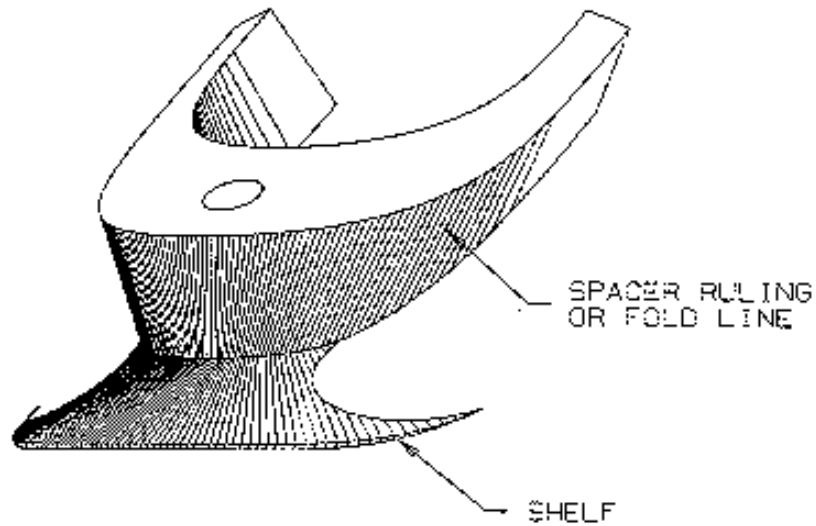


Figure 5: An end part with shelf as an integral part (from J. Brandt).

However, as part of the VLHC program efforts to bring down the overall cost of such a machine, efforts are underway to investigate alternative manufacturing technologies to reduce the cost of end parts fabrication. Therefore, we are investigating waterjet machining as an alternative to the conventional 5-axis milling operation. Abrasive

waterjet machining has a significant advantage of reducing both the cost and the time of end parts fabrication. It also offers the opportunity to use ceramic materials¹ for end parts fabrication. However, we can not use shelves with this technique. One way to get around this is to use smaller final edge angles than that suggested by program BEND based upon the strain-energy minimization concepts. It should be noted that by using smaller inclination (or final edge) angles, we want to avoid large radial gaps that can occur in conductor groups if we use large inclination angles but no shelves to fill the extra radial space. Since the high field magnet coils get epoxy impregnated, epoxy would fill any gaps that are present. This epoxy could then crack at cryogenic temperatures leading to possible quenches at the magnet ends.

A study was conducted at Fermilab to investigate the effect of changing the inclination (final edge) angle of the conductor groups. Two practice coils were wound. Tables 1-4 provide the conductor inclination angles used for the two practice coils. Also shown in these Tables are the conductor inclination angles suggested by program BEND based upon the strain-minimization principles. The first practice coil (PC02) had larger deviation in conductor inclination angles from the values suggested by program BEND than the second practice coil (PC03). Also, the first practice coil was wound using aluminum bronze end parts that were fabricated using a wire EDM. In an effort to reduce the cost of R&D for the practice coils, the second practice coil was wound using parts made of copper-duraform that were fabricated using a cheap and fast rapid prototyping technique - the selective laser sintering (SLS²) technology. Figures 6 and 7 show a comparison of the quality of the return end cross-section for the two practice coils. Similar comparison for the lead end cross-section is presented in Figures 8 and 9. Figures 10 to 43 show a blow up of each of the conductor groups for the two practice coils.

It is clear from these figures that the practice coil, PC03 has a much better end quality than the practice coil, PC02. This suggests that although some deviation (as in PC03) from the inclination angle value suggested by program BEND is acceptable, large deviation (as in PC02) in conductor inclination angle leads to poor quality ends. We would let the accompanying figures (Fig. 10-43) illustrate this effect further.

¹ The end parts for the high field magnets are required to sustain high Nb₃Sn cable reaction temperature (~650-700 °C). The current material of choice is bronze due to its non-magnetic properties and high melting temperature. However, the use of metal end parts requires either coating the end parts with an electrically insulating (ceramic) coating or relying on the strong cable insulation. Since ceramics are electrically insulating, their use can increase the magnet reliability. However, further considerations need to be made to study thermo-mechanical properties of the ceramics.

² SLS is a rapid prototyping technique that uses powder to make prototype parts. The powder is melted, layer by layer, by a computer-directed heat laser. Additional powder is deposited on top of each solidified layer and again sintered. The advantage of this technology is that the parts can be made at a very economical price and in a very short time using solid models of the parts created in solid modeling program such as SDRC's I-DEAS. We have further developed a program file in I-DEAS that can read output data from BEND and generate solid models of all the different end parts automatically.

Reference

- [1] O. Grobner, "The LHC vacuum system," *Proc. of CERN Accelerator School on Vacuum Technology*, Scanticon Conference Center, Snekersten, Denmark, pp. 291-306, June 1999.
- [2] P. Bauer, C. Darve, T. Peterson, and B. Jenninger, "Very large hadron collider beam screen design-preliminary investigation of space requirement," Fermilab Technical Division Note TD-99-032, 1999.
- [3] J. M. Cook, "An application of differential geometry to SSC magnet end winding," Fermilab Technical Division Note TM-1663, 1990.
- [4] J. M. Cook, "Strain energy minimization in SSC magnet winding," *IEEE Trans. on Magnetics*, vol. 27, pp. 1976-1980, Mar. 1991.
- [5] J. Brandt, N. Bartlett, R. Bossert, et al., "Coil end design for the SSC collider dipole magnet," Fermilab-TM-1735, July 1991.
- [6] R.C. Bossert, J.S. Brandt, et al., "Construction experiences with SSC collider dipole magnets at Fermilab," *IEEE Transactions on Magnetics*, Vol. 28, pp. 129-132, January 1992.

Table 1: Comparison of conductor inclination angles for inner layer, return end conductor groups for practice coils # 02 and 03 versus the values suggested by program BEND.

CONDUCTOR GROUP	BEND	PC02	PC03
IR1	16.8	16.8	16.8
IR2	32.4	25	25
IR3	40.8	20	25

Table 2: Comparison of conductor inclination angles for outer layer, return end conductor groups for practice coils # 02 and 03 versus the values suggested by program BEND.

CONDUCTOR GROUP	BEND	PC02	PC03
OR1	28.9	15	20
OR2	36.3	15	25
OR3	42.6	10	25

Table 3: Comparison of conductor inclination angles for inner layer, lead end conductor groups for practice coils # 02 and 03 versus the values suggested by program BEND.

CONDUCTOR GROUP	BEND	PC02	PC03
IL1	20.1/16.8	16.8	20
IL2	35/21.8	25	25
IL3	32.4/34.6	25	25
IL4	41.9/37.1	25	25
IL5	41.7/40.8	25	25

Table 4: Comparison of conductor inclination angles for outer layer, lead end conductor groups for practice coils # 02 and 03 versus the values suggested by program BEND.

CONDUCTOR GROUP	BEND	PC02	PC03
OL1	17.3/28.9	14.1	20
OL2	28.93/31.44	20	20
OL3	31.44/43.4	15	20
OL4	36.3/38.3	15	25
OL5	40.4/47	10	25
OL6	42.6/43.8	10	25

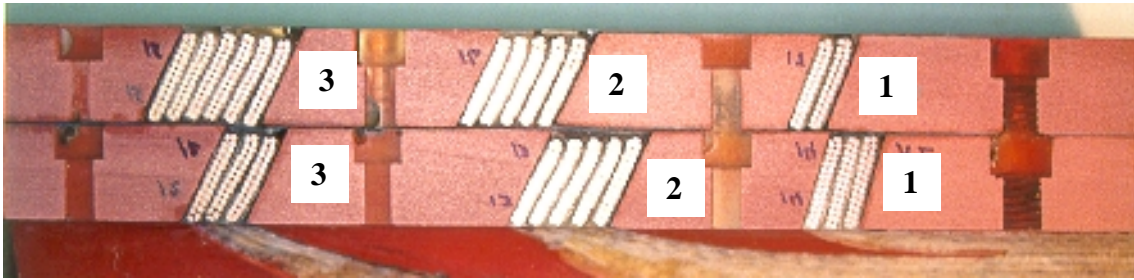


Figure 6: Return end cross-section for practice coil # 03 showing different conductor groups.

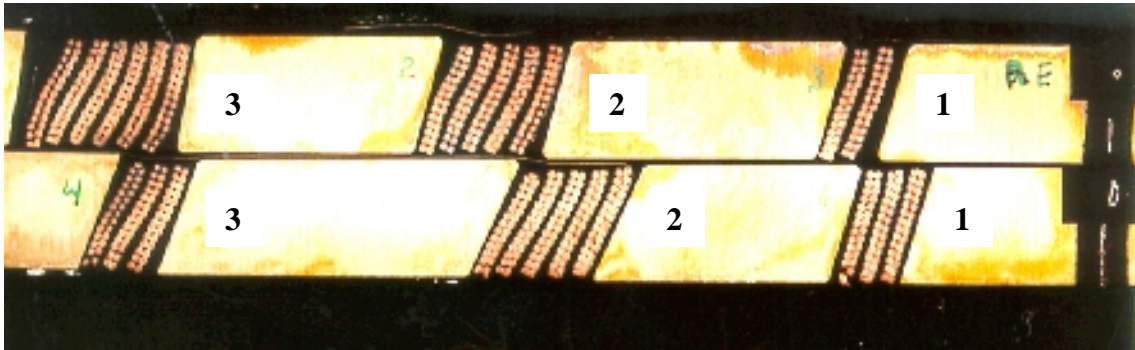


Figure 7: Return end cross-section for practice coil # 02 showing different conductor groups.

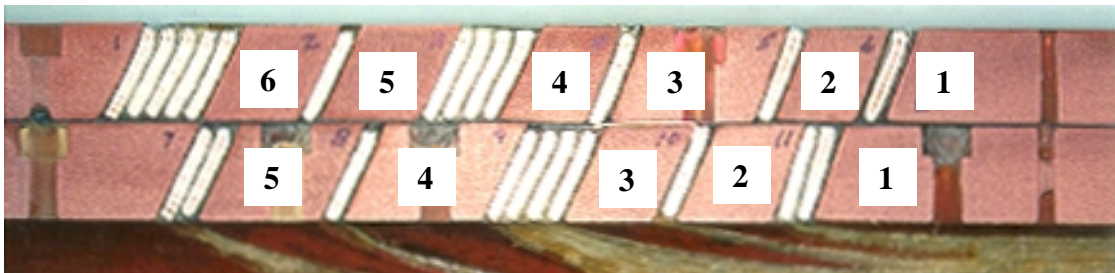


Figure 8: Lead end cross-section for practice coil # 03 showing different conductor groups.

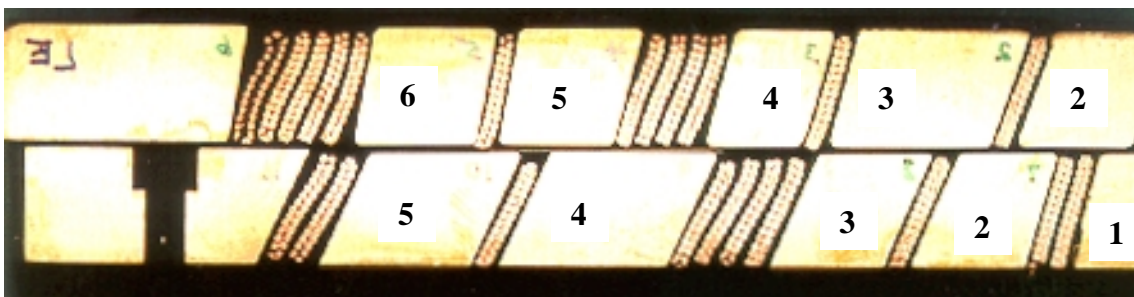
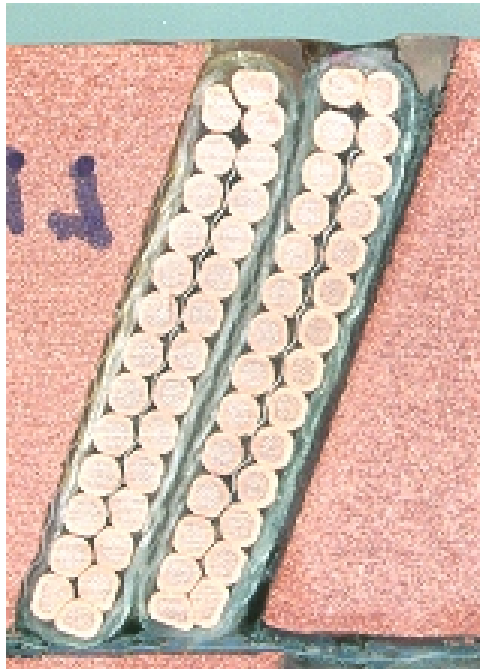


Figure 9: Lead end cross-section for practice coil # 02 showing different conductor groups.

RETURN END-OUTER LAYER

CONDUCTOR GROUP 1



(20°/28.9°)

Figure 10: Return end, outer layer, conductor group 1 cross-section for practice coil # 03.



(15°/28.9°)

Figure 11: Return end, outer layer, conductor group 1 cross-section for practice coil # 02.

CONDUCTOR GROUP 2



(25°/36.3°)

Figure 12: Return end, outer layer, conductor group 2 cross-section for practice coil # 03.



(15°/36.3°)

Figure 13: Return end, outer layer, conductor group 2 cross-section for practice coil # 02.

CONDUCTOR GROUP 3



(25°/42.6°)

Figure 14: Return end, outer layer, conductor group 3 cross-section for practice coil # 03.

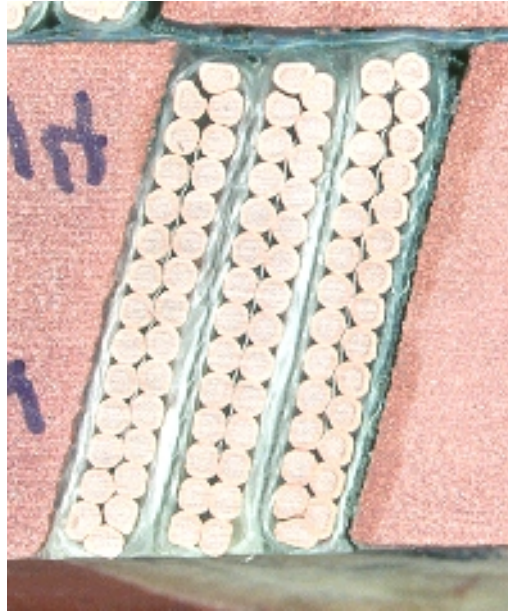


(10°/42.6°)

Figure 15: Return end, outer layer, conductor group 3 cross-section for practice coil # 02.

RETURN END-INNER LAYER

CONDUCTOR GROUP 1



(16.8°/16.8°)

Figure 16: Return end, inner layer, conductor group 1 cross-section for practice coil # 03.



(16.8°/16.8°)

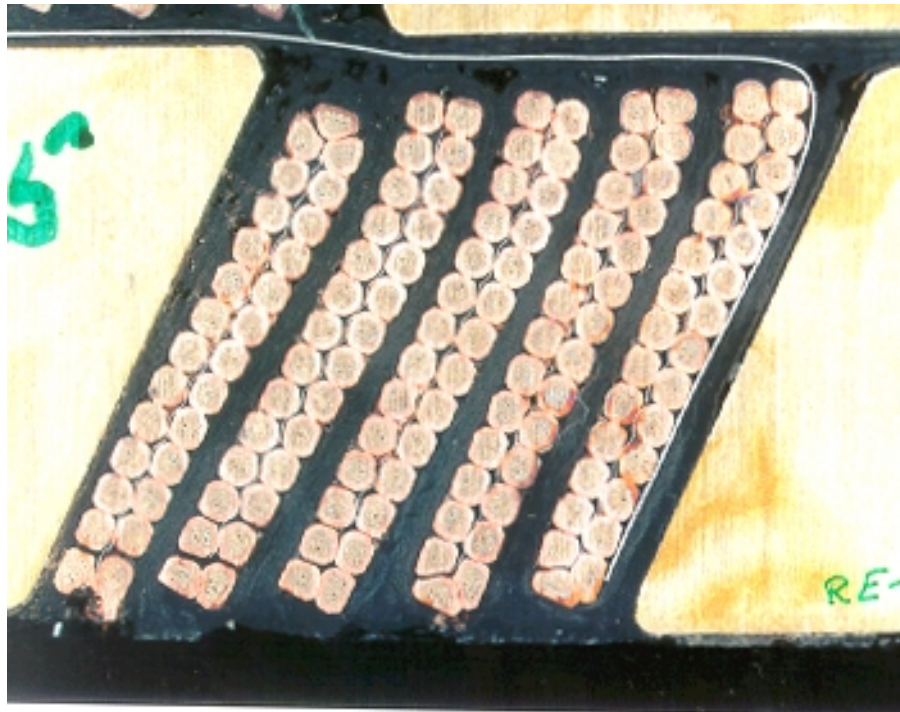
Figure 17: Return end, inner layer, conductor group 1 cross-section for practice coil # 02.

CONDUCTOR GROUP 2



(25°/32.4°)

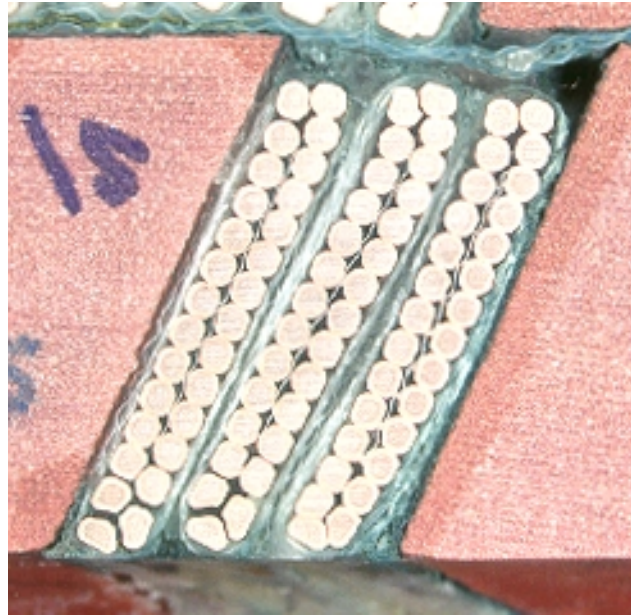
Figure 18: Return end, inner layer, conductor group 2 cross-section for practice coil # 03.



(25°/32.4°)

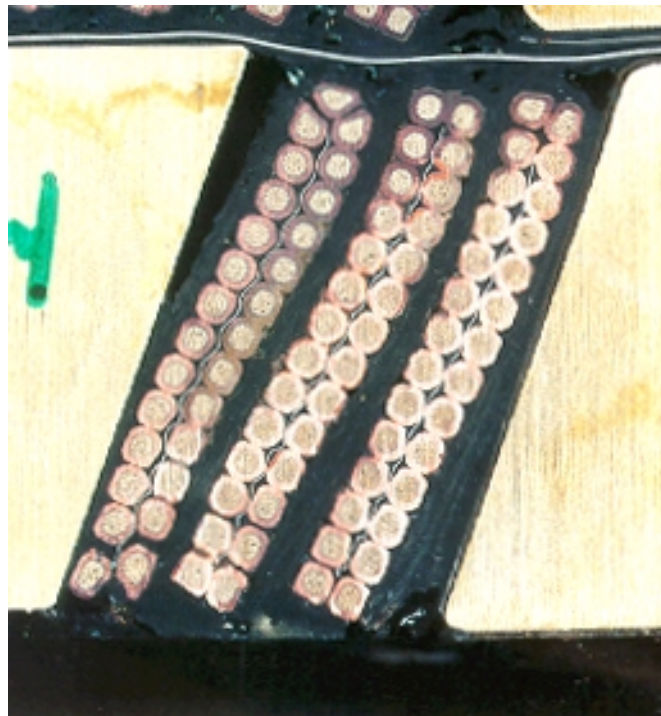
Figure 19: Return end, inner layer, conductor group 2 cross-section for practice coil # 02.

CONDUCTOR GROUP 3



(25°/40.8°)

Figure 20: Return end, inner layer, conductor group 3 cross-section for practice coil # 03.



(20°/40.8°)

Figure 21: Return end, inner layer, conductor group 3 cross-section for practice coil # 02.

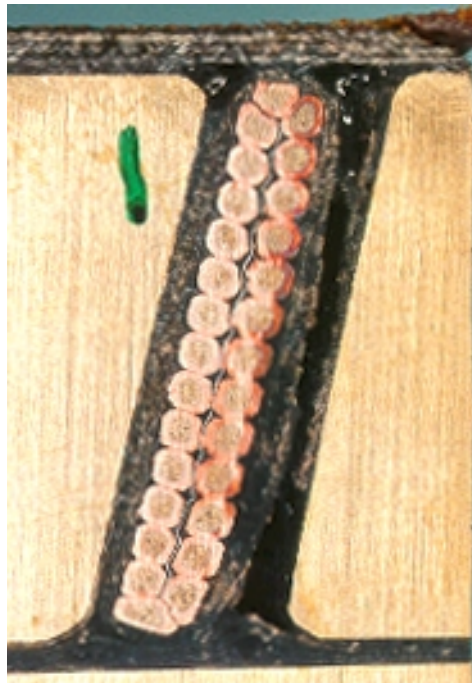
LEAD END-OUTER LAYER

CONDUCTOR GROUP 1



(20°/17.3° & 28.9°)

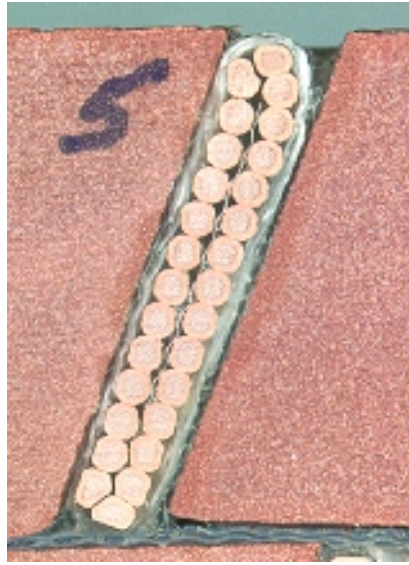
Figure 22: Lead end, outer layer, conductor group 1 cross-section for practice coil # 03.



(14.1°/17.3° & 28.9°)

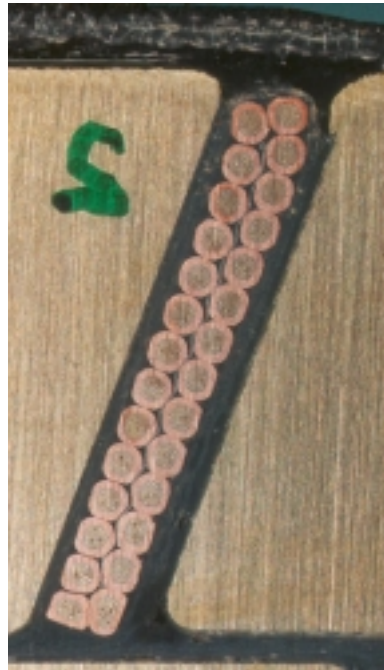
Figure 23: Lead end, outer layer, conductor group 1 cross-section for practice coil # 02.

CONDUCTOR GROUP 2



(20°/28.9° & 31.4°)

Figure 24: Lead end, outer layer, conductor group 2 cross-section for practice coil # 03.



(20°/28.9° & 31.4°)

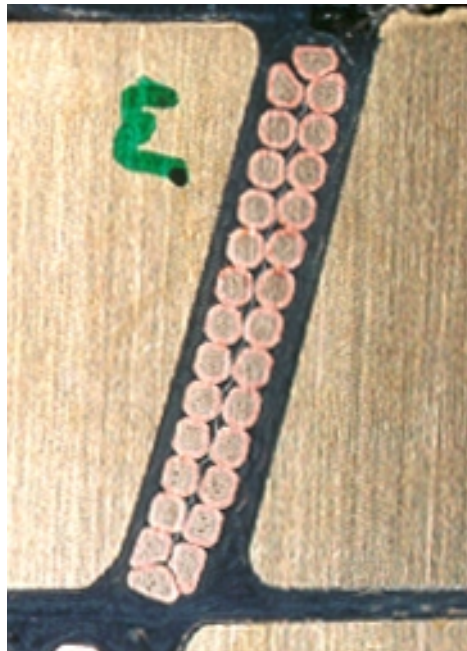
Figure 25: Lead end, outer layer, conductor group 2 cross-section for practice coil # 02.

CONDUCTOR GROUP 3



(20°/31.4° & 43.4°)

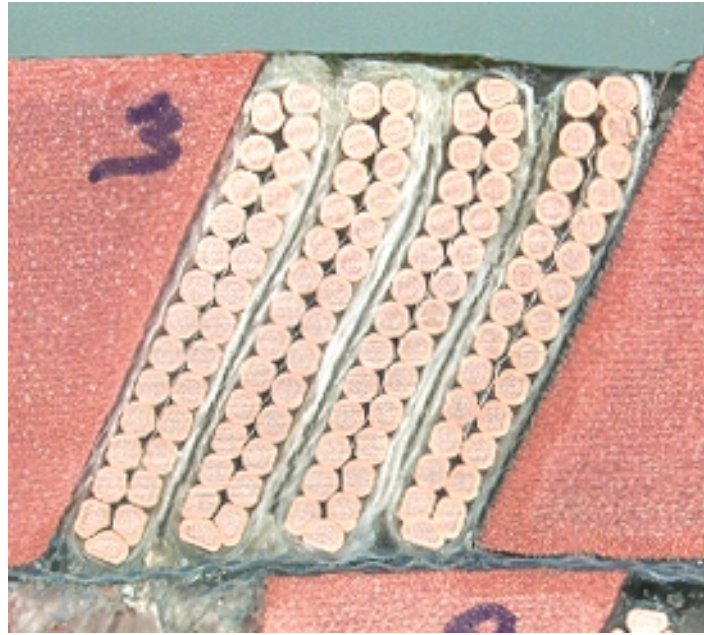
Figure 26: Lead end, outer layer, conductor group 3 cross-section for practice coil # 03.



(15°/31.4° & 43.4°)

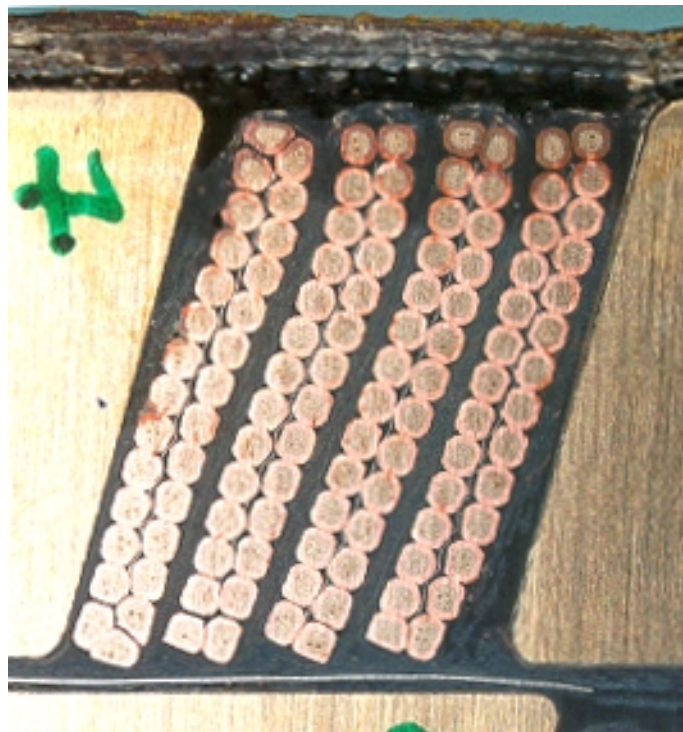
Figure 27: Lead end, outer layer, conductor group 3 cross-section for practice coil # 02.

CONDUCTOR GROUP 4



(25°/36.3° & 38.3°)

Figure 28: Lead end, outer layer, conductor group 4 cross-section for practice coil # 03.



(15°/36.3° & 38.3°)

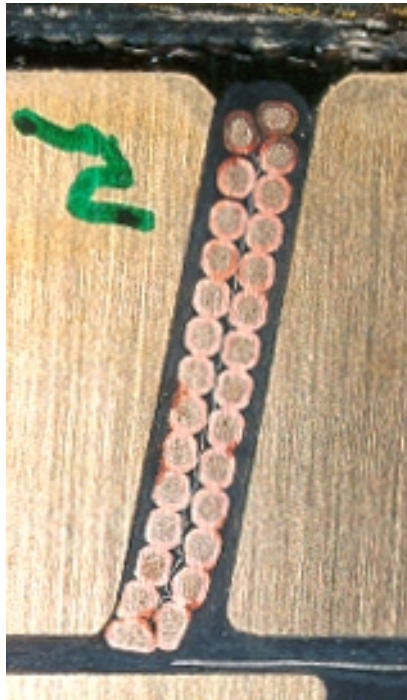
Figure 29: Lead end, outer layer, conductor group 4 cross-section for practice coil # 02.

CONDUCTOR GROUP 5



(25°/40.4° & 47°)

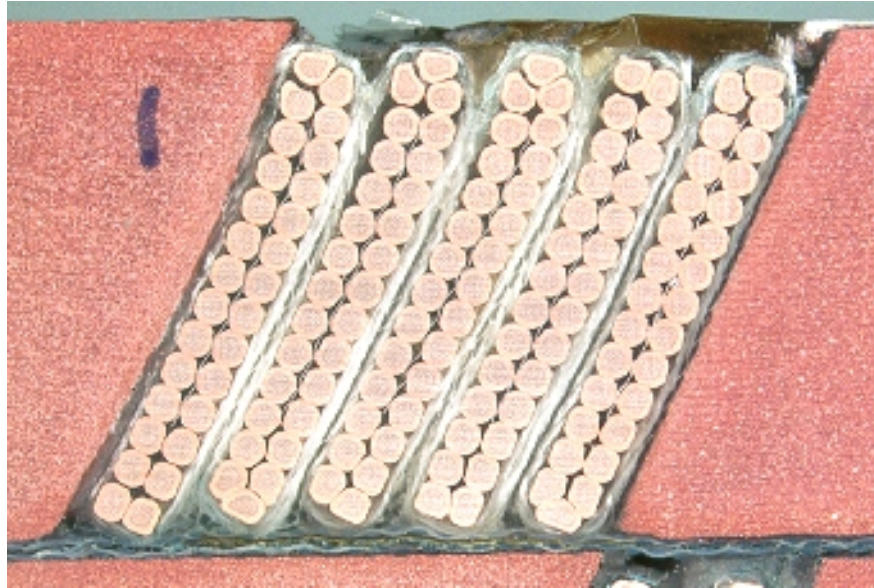
Figure 30: Lead end, outer layer, conductor group 5 cross-section for practice coil # 03.



(10°/40.4° & 47°)

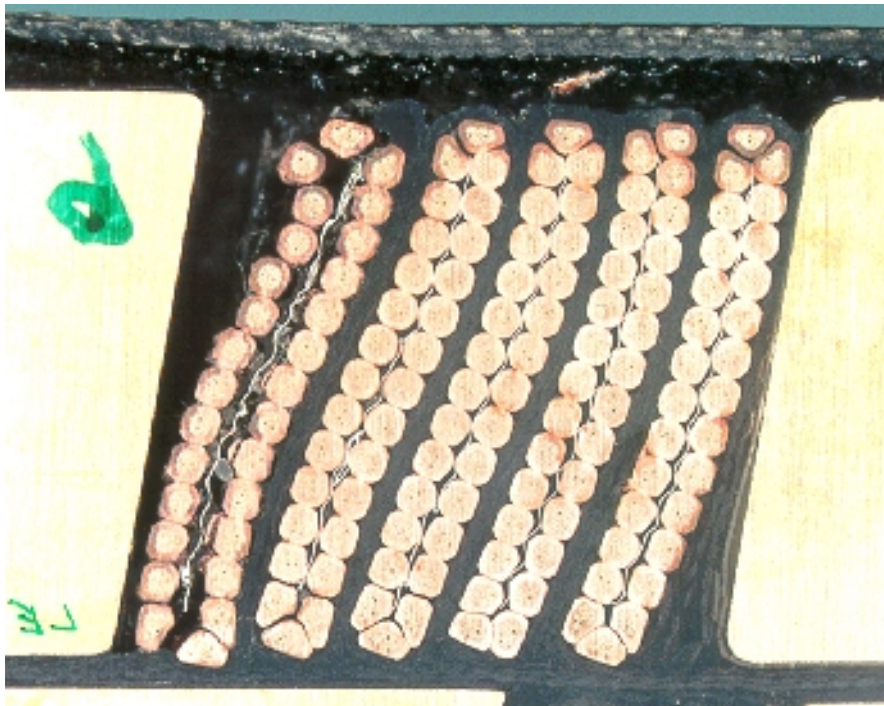
Figure 31: Lead end, outer layer, conductor group 5 cross-section for practice coil # 02.

CONDUCTOR GROUP 6



(25°/42.6° & 43.8°)

Figure 32: Lead end, outer layer, conductor group 6 cross-section for practice coil # 03.

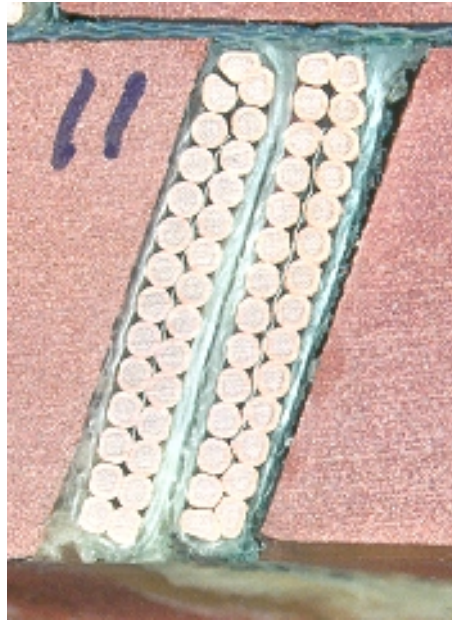


(10°/42.6° & 43.8°)

Figure 33: Lead end, outer layer, conductor group 6 cross-section for practice coil # 02.

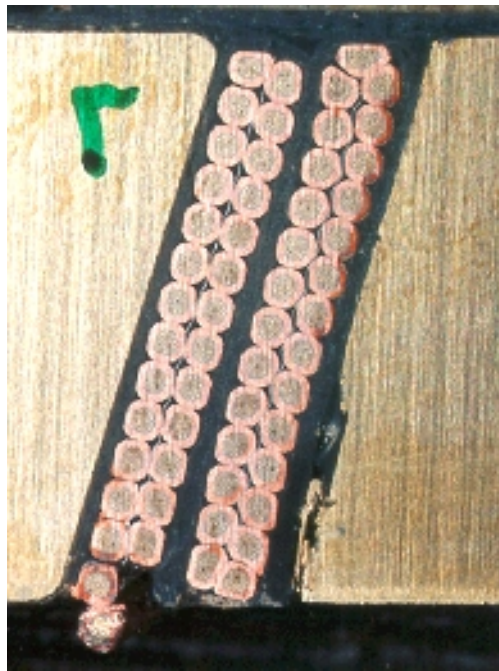
LEAD END-INNER LAYER

CONDUCTOR GROUP 1



(20°/20.1° & 16.8°)

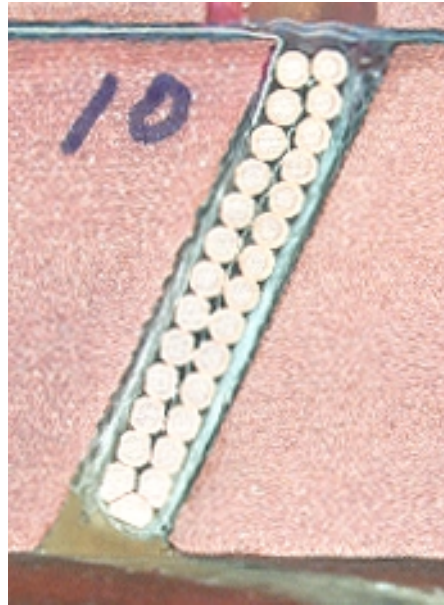
Figure 34: Lead end, inner layer, conductor group 1 cross-section for practice coil # 03.



(16.8°/20.1° & 16.8°)

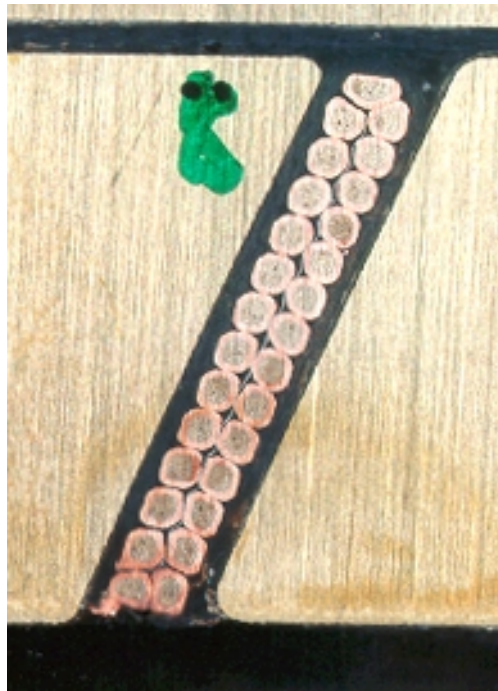
Figure 35: Lead end, inner layer, conductor group 1 cross-section for practice coil # 02.

CONDUCTOR GROUP 2



(25°/35° & 21.8°)

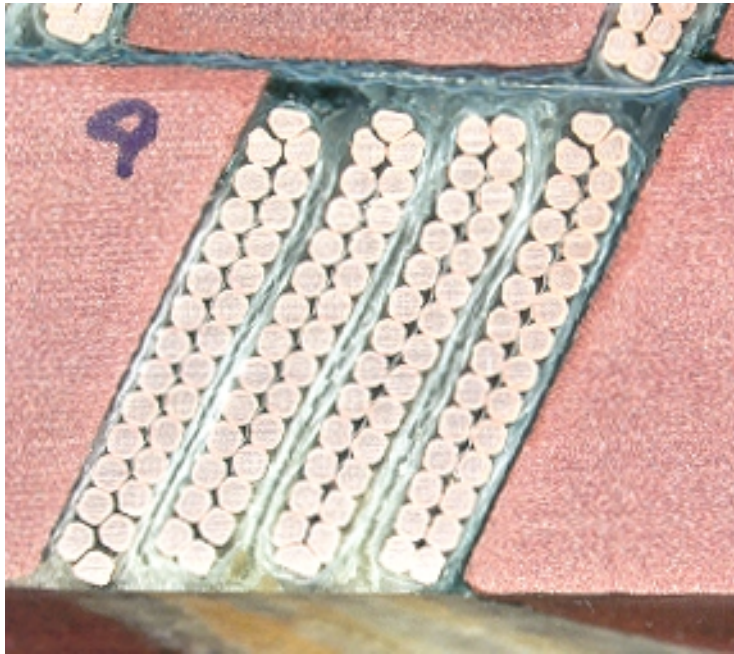
Figure 36: Lead end, inner layer, conductor group 2 cross-section for practice coil # 03.



(25°/35° & 21.8°)

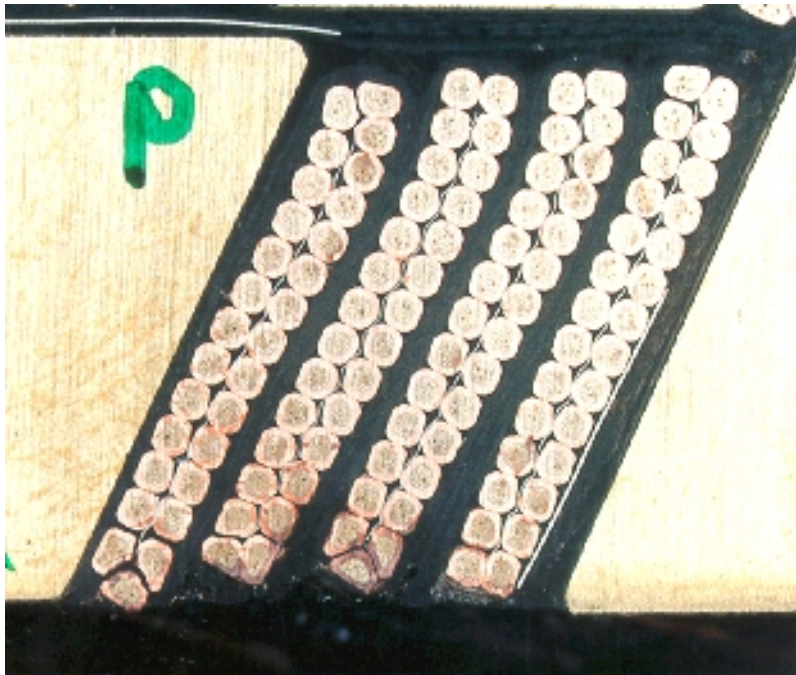
Figure 37: Lead end, inner layer, conductor group 2 cross-section for practice coil # 02.

CONDUCTOR GROUP 3



(25°/34.6° & 32.4°)

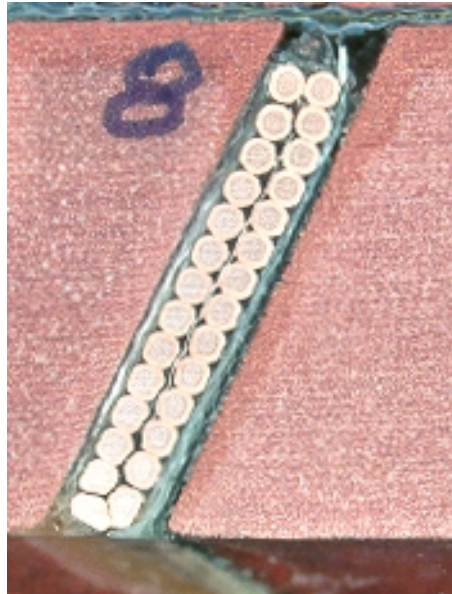
Figure 38: Lead end, inner layer, conductor group 3 cross-section for practice coil # 03.



(25°/34.6° & 32.4°)

Figure 39: Lead end, inner layer, conductor group 3 cross-section for practice coil # 02.

CONDUCTOR GROUP 4



(25°/41.9° & 37.1°)

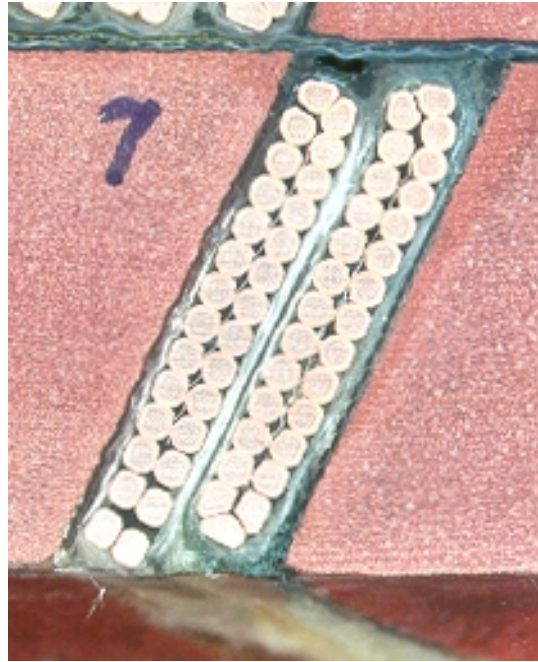
Figure 40: Lead end, inner layer, conductor group 4 cross-section for practice coil # 03.



(25°/41.9° & 37.1°)

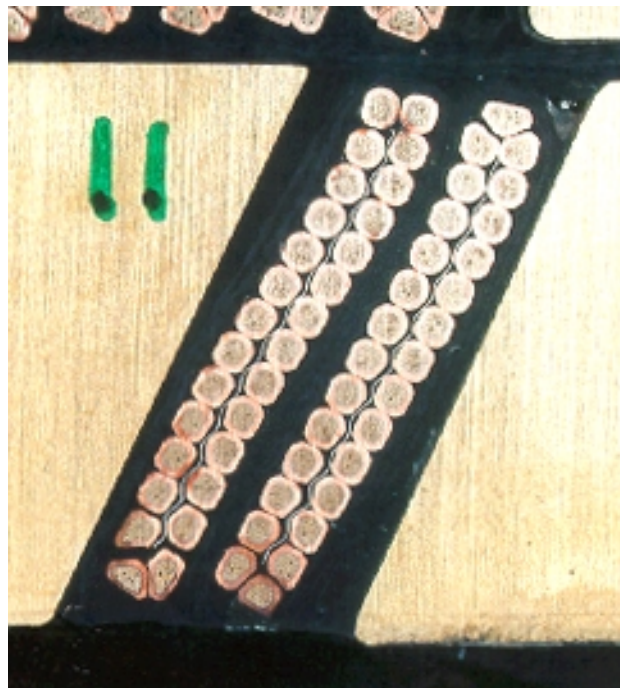
Figure 41: Lead end, inner layer, conductor group 4 cross-section for practice coil # 02.

CONDUCTOR GROUP 5



(25°/41.7° & 40.8°)

Figure 42: Lead end, inner layer, conductor group 5 cross-section for practice coil # 03.



(25°/41.7° & 40.8°)

Figure 43: Lead end, inner layer, conductor group 5 cross-section for practice coil # 02.